Unsupported trimetallic Ni(Co)-Mo-W sulphide catalysts prepared from mixed oxides: characterisation and catalytic tests for simultaneous tetralin HDA and dibenzothiophene HDS reactions

Unsupported trimetallic Ni(Co)-Mo-W sulphide catalysts prepared from mixed oxides: characterisation and catalytic tests for simultaneous tetralin HDA and dibenzothiophene HDS reactions

Yordy E. Licea,*[a,c] Ricardo Grau-Crespo,[b] Luz A. Palacio[c] and Arnaldo C. Faro Jr.[a]

[a] Instituto de Química, Universidade Federal de Rio de Janeiro, Av. Athos da Silveira Ramos, 149 Bloco A, CEP, 21941-909, Rio de Janiero, RJ, Brasil.

[b] Department of Chemistry, University of Reading, Whiteknights, Reading RG6 6AD, UK.

[c] Instituto de Química, Universidade do Estado de Rio de Janeiro, Rua São Francisco Xavier, 524, CEP, 20550-900, Rio de Janeiro, RJ, Brasil.

*Corresponding author. E-mail address: yliceafonseca@gmail.com *Current Address: CENANO-DCAP, Instituto Nacional de Tecnologia. Av. Venezuela 82, CEP: 20081-312, Rio de Janeiro, RJ, Brasil

Abstract

Unsupported A-Mo-W (A = Ni or Co) sulphide catalysts were obtained from mixed oxides containing different W:Mo ratios. An *in situ* liquid-phase sulphidation of the mixed oxides in a batch reactor was followed by catalytic tests in a liquid-phase reaction (at 613 K and 70 bar), using a mixture of dibenzotiophene (DBT) and tetralin (THN) as the feed. After the catalytic tests, the bulk sulphide catalysts were characterised by nitrogen physical adsorption, XANES/EXAFS, SEM and HR-(S)TEM. The HR-TEM images showed randomly oriented, stacked-layer particles typical of Mo (W) sulphides and an elemental HR-STEM mapping evidenced Mo/W homogeneous distribution in the trimetallic sulphides. The EXAFS results for the trimetallic catalysts are consistent with the presence of nickel or cobalt sulphide

domains, and $Mo_{1-x}W_xS_2$ solid solutions. The intralayer Mo:W solid solutions were confirmed to be thermodynamically stable with respect to phase separation by DFT calculations, which were also used to aid in the interpretation of the EXAFS results. The effect of the W:Mo ratio on the catalytic properties of the Ni- and Co-containing series was found to be different. For the Ni series, increasing the W content caused an activity increase in THN hydrodearomatization (HDA) relative to DBT hydrodesulphurization (HDS), while it had little influence on the relative contribution of the *direct desulphurisation* (DDS) route with respect to the *previous hydrogenation* (HYD) route for DBT HDS. In contrast, for the Co series, the activities and selectivities were essentially insensitive to the W content. Both the Ni and Co series of unsupported sulphides were more selective for the HYD route in DBT HDS than a supported $NiMo/Al_2O_3$ catalyst.

Keywords: hydrotreating, trimetallic bulk sulphides, hydrodearomatization, disorder solid solutions

1. Introduction

Hydrotreating processes are used in oil refineries for reducing the content of unwanted components (such as sulphur, nitrogen and metal compounds, as well as aromatic hydrocarbons) in oil fractions and products, by reaction with hydrogen. Due to the tightening of air-quality legislation in many countries [1], there is a continuing effort to develop more efficient catalysts and processes for the production of ultralow-sulphur fuels, especially diesel (USLD). Although great progress has been made in the development of efficient catalysts for these processes, major challenges remain, for example, their modest aromatic hydrocarbons saturation activity. Improving the aromatics saturation activity of hydrotreating catalysts has become a research priority since recent environmental restrictions establish minimum values

for cetane number and lower limits for polyaromatic contents in diesel cuts.

Unsupported catalysts have emerged as a promising commercial alternative to fulfil tighter diesel specifications, without the need for an extensive revamp of existing refinery hydrotreating units [2, 3]. This is due to their higher hydrogenating power, even if they are generally more expensive than conventional supported catalysts because of their larger metal content. In the last decade, since the first patents for their use in hydrotreating were published (e.g. [4]), the interest in the study of trimetallic (NiMoW) sulphides has considerably increased [2, 5].

Previous research [6-11], using thiosalts for the preparation of unsupported bimetallic sulphide catalysts, has led to significant progress in the understanding of their structure and catalytic activity. Thomazeau et al. [12] synthesised bulk $Mo_{1-x}W_xS_2$ compounds from thiosalts, and used EXAFS to show that Mo and W cations were present in every sulphide layer, *i.e*, intralayer solid solutions were formed. Later work by the same authors [13] showed that the $Mo_{0.5}W_{0.5}S_2$ system kept the intralayer solid solution structure when it was supported on alumina (by a co-precipitation method) and subsequently nickel-doped. The catalytic activity of these samples was evaluated in gas-phase thiophene hydrodesulphurization (HDS) and in liquid-phase HDS of a hydrotreated gasoil [14]. Based on DFT calculations of (unsupported) cluster systems, the ternary $NiMo_{1-x}W_xS_2$ compounds were expected to be more active than the bimetallic NiW and NiMo sulphides, in contrast with the $CoMo_{1-x}W_xS_2$ system where no Mo/W synergy was predicted. The catalytic activities of the promoted $NiMo_{1-x}W_xS_2$ unsupported systems were not reported in that work.

Unfortunately, the preparation of hydrotreating catalysts from thiosalts is difficult to scale up [15], due to the costs involved and the use of toxic ammonium sulphide or hydrogen sulphide in the preparation of the precursors. It is therefore surprising that little attention has been paid

to the preparation of trimetallic unsupported hydrotreating catalysts from oxide-precursors [16, 17], which is a relatively cheaper and easier method.

Well-characterised Ni-promoted $Mo_{1-x}W_xS_2$/ Al_2O_3 catalysts with different Mo to W ratios were synthesised by pore volume impregnation of γ-Al_2O_3 with the metal salts in a recent work by van Haandel et al. [18]. There was no synergy from the simultaneous presence of Mo and W in ternary Ni-based $Mo_{1-x}W_xS_2$ materials under the reported conditions of the model reactions, either in the gas-phase thiophene HDS or in the liquid-phase dibenzothiphene (DBT) HDS activity. The effect of pressure and temperature in the gas-phase catalyst activation was followed by XPS and EXAFS. The mixing of W and Mo in the $Mo_{1-x}W_xS_2$ slabs was found to be dependent on the activation pressure in those supported systems. At higher activation pressures a Mo-W solid solution was formed whereas, for lower activation pressure, EXAFS gave evidence of Mo-W-S sulphide particles with a core-shell structure.

There is clearly a lack of information in the open literature about the physicochemical and catalytic properties of bulk trimetallic NiMoW sulphides prepared from mixed oxides and virtually no information on the related CoMoW system. Furthermore, most model compound studies reported for unsupported catalysts involve only the HDS reaction (DBT and/or 4,6-dimethyldibenzothiophene [15, 19-24]. However, as mentioned earlier, there is currently much interest in the HDA function of hydrotreating catalysts [25], so it is important to make catalytic measurements in the simultaneous HDS of sulphur compounds and the HDA of aromatic hydrocarbons [26-29].

Hein et al. [30] studied unsupported bimetallic catalysts with Ni/Mo=1.2 and Ni/W=0.9, and an unsupported trimetallic catalyst with Ni/(Mo+W)=1.3. These Ni-based precursors, not characterised in that work, were sulphided in the gas phase without previous thermal

treatment. The catalysts activities were evaluated for the hydrodenitrogenation (HDN) of *o*-propylaniline and HDS of DBT. The trimetallic catalyst had both greater HDN and HDS activities than the bimetallic ones. The authors explained this result by the preferential incorporation of Ni in the perimeter of the mixed trimetallic $Mo_{1-x}W_xS_2$ slabs. Only the trimetallic catalyst with Mo/W=1.3 was studied, no other Mo/W ratios were considered. Co-based catalysts were not studied in that work.

Recently Licea et al. [31] have investigated the properties of NiMo bulk sulphide catalysts obtained from mixed oxides. The mixed oxides were obtained by calcining a synthesised lamellar precursor with the so-called ϕ_y phase, whose crystal structure has been determined by Ying et al. [31], with general formula $(NH_4)H_{2x}Ni_{3-x}(OH)_2(MoO_4)_2$ ($0 \leq x \leq 3/2$). Ni atoms can fractionally occupy the octahedral sites, which allows the synthesis of compounds with Ni/Mo ratios in the range from 0.75 to 1.5. Layered structures containing Co, Cu or Zn as the divalent metal have also been reported [32] but despite the chemical similarities of W and Mo [33], these ϕ_y structures containing W atoms have not been reported so far in the open literature.

It is well known that DBT undergoes HDS by two parallel paths, namely the *direct desulphurization* (DDS) and the *previous hydrogenation* (HYD) routes [34]. In the work of Licea et al. [31] the mixed oxides were *in situ* sulphided and the catalytic activity of the mixed sulphides was evaluated in the simultaneous dibenzothiophene (DBT) HDS and tetrahydronaphthalene (THN) HDA reactions. The NiMo bulk sulphide displayed pronounced selectivity for the HYD pathway in DBT HDS, when compared to a conventional NiMo alumina-supported catalyst. This is known to be the pathway that benefits the HDS reaction of the most refractory organo-sulphur molecules (alkyl-dibenzothiophenes) under hydrotreating conditions [25, 35].

In the present work, Ni-Mo-W catalysts and Co-Mo-W bulk sulphides were prepared from liquid-phase sulphidation of mixed-oxide precursors. The activity and selectivity of the catalysts were evaluated in the sulphided state in the simultaneous HDS of dibenzothiophene (DBT) and HDA of tetralin (tetrahydronaphtalene, THN) and were further characterised by several physicochemical techniques. A combination of EXAFS and density functional theory calculations was employed to investigate the mixed MoW sulphides, in particular to establish whether or not solid solutions were obtained by the preparation method used, and if formed, whether the solid solutions were ordered or disordered.

2. Experimental

2.1. Synthesis

Two series of AMoW (A = Ni or Co) precursors were synthesised by a co-precipitation method as described elsewhere [31]. Ammonium heptamolybdate and ammonium metatungstate aqueous solutions were prepared each containing quantities of Mo and W to obtain 1:0, 2:1, 1:1, 1:2 and 0:1 molar Mo:W solutions. A Ni (or Co) nitrate aqueous solution was also prepared so to obtain equimolar A: (Mo+W) compounds. By the slow addition of NH_4OH, the pH of the solution was increased to 8. The solution was then transferred to a closed bottle, where a treatment was carried-out for 4 hours at 353 K. The Ni-based green (yellowish for some compounds) and Co-based pink (brown for some compounds) precipitates obtained were then washed with enough water to reach neutral pH and then dried for 24 hours. The synthesised ammonia-containing materials were nominated A_z-Mo_y-W_x-am, where "am" stands for ammonia, A=Ni or Co, z is the A/(W+Mo) molar ratio, x is the W/(Mo+W) molar ratio, and y=1-x is the Mo/(Mo+W) molar ratio. The values of z and x were obtained from the X–ray fluorescence (XRF) chemical analysis of the samples (*c.f* Table 1). In order to simplify the notation, the materials not containing W were denominated

$Ni_{1.6}$-Mo-am and $Co_{1.1}$-Mo-am, whereas the materials not containing Mo were denominated $Ni_{1.6}$-W-am and $Co_{1.2}$-W-am.

In order to obtain the mixed oxides, the Ni-based and Co-based precursors were heated under static air at a rate of 5 K min^{-1} up to 673 K and 623 K, respectively, and maintained at the final temperature for 3 h. The calcination temperatures were chosen as low as possible to maximise the surface areas, while also guaranteeing that all volatile compounds (H_2O and NH_3) were evolved, based on the thermogravimetric analysis of the precursors. The corresponding calcined materials were named A_z-Mo_y-W_x-ca ("ca" stands for calcined). The sulphidation was performed *in-situ*, immediately before the catalytic tests, as described under section 2.8, and the sulphide catalysts were named A_z-Mo_y-W_x-s ("s" stands for sulphide). It should be emphasised that in all cases the subscripts *x*, *y*, *z* represent the overall compositions of the samples and do not imply the existence of single phases with the given stoichiometry.

The NiMo layered precursor ($Ni_{1.6}$-Mo-am), its corresponding mixed oxide ($Ni_{1.6}$-Mo-ca) and sulphided catalyst ($Ni_{1.6}$-Mo-s) have been studied in previous work [31], where the simultaneous HDS/HDA activity of the latter was compared with that of an alumina-supported NiMo material synthesised in our laboratory [36].

2.2. Elemental analysis

A Rigaku RIX 2100 instrument with a rhodium tube operated at 4 kW was used for analysis of the metals by X-ray fluorescence (XRF). The samples were analyzed as ca. 600 mg wafers, after calcination at 823 K.

2.3. X-Ray diffraction

X-ray powder diffraction (XRD) patterns for the layered precursors and mixed oxides were obtained in a Rigaku Ultima IV apparatus using CuK_α radiation (λ=0.15418 nm), operated at 40 kV and 20 mA. Scans were performed at 2º min^{-1} in the 3º to 70º range in steps of 0.02º.

2.4. Textural properties

The textural characterisation of both the calcined and the sulphided materials using nitrogen physisorption was made using a Micromeritics ASAP 2010 C equipment. Both the calcined and the sulphided samples were pretreated in-situ at 473 K under vacuum before the analyses. Surface areas were determined using the BET method and pore size distributions were obtained using the BJH method [37] from the adsorption branch of the isotherms.

The sulphided catalysts were analysed after the catalytic tests. The samples soaked with the reaction mixture were washed first with toluene, then with n-hexane. While soaked in n-hexane, they were placed in a Schlenk flask and heated under N_2 flow (30 cm^3/min) for 4 h at 573 K in order to eliminate the solvent. Under the same flow, the samples were cooled down to room temperature and then the nitrogen flow was switched to a 0.5% O_2/N_2 (~80 cm^3 min^{-1}) gas mixture during 4h for surface passivation. The powder was then transferred to the ASAP sample cell, where it was heated under vacuum at 473 K and then analysed.

2.5. Electron Microscopy

A FEI Inspect F50 scanning electron microscope, a JEOL transmission electron microscope (TEM-FEG) JEM 2100F and a TEM-HR JEOL 3010 microscope (all located at the Brazilian Nanotechnology National Laboratory in Campinas, Sao Paulo), were used for microscopy studies.

The $Ni_{1.7}$-$Mo_{0.50}$-$W_{0.50}$ and $Co_{1.3}$-$Mo_{0.41}$-$W_{0.59}$ surfaces were covered by sputtered Au films (~16 nm) before they were placed in the sample holder for particle morphology studies in the Inspect microscope. STEM images using a Thermo-Noran scanning image observation device (STEM) and an ASID control operation STEM mode was used for the elemental mapping characterisation of the sulphided $Ni_{1.7}$-$Mo_{0.50}$-$W_{0.50}$-s and $Co_{1.3}$-$Mo_{0.41}$-$W_{0.59}$-s

catalysts at 200 kV. For the HR-TEM images (300 kV) the catalyst samples were first washed and then ultrasonicated in ethanol before some drops were placed onto a carbon-coated copper grid.

2.6. XAS measurements

X-ray absorption spectra were taken at XAFS1 or XAFS2 beamlines at the Brazilian Synchrotron Light Laboratory (LNLS), Campinas, Brazil, operated at 1.37 GeV with a maximum beam current of 250 mA. The analyses were carried-out in the ranges from 7580-8300 eV, 8230-9600 eV, 19900-21300 eV and 10100-11300 eV for Ni-K, Co-K, Mo-K and W-L_3 edges acquisition, respectively. A metal Co, Ni, Mo or W foil was used for energy calibration reference in the respective cases. The EXAFS spectra were analysed by standard procedures of data reduction using the IFEFFIT code [38]. Structural parameters were obtained from least squares fitting in R-space. The amplitude functions were obtained theoretically from the FEFF8.2 program [39] in the case of the CoS and experimentally for MoS_2, WS_2 and Ni_3S_2. The parameters optimised by the software were defined as usual, except in the trimetallic sulphided catalysts where a simultaneous simulation using the EXAFS W L_3- and Mo K-edge were used, as explained below. XANES in the Mo L_3-edge energy region spectra were taken at the SXS beamline at LNLS for both A_z-Mo_y-W_x-am precursors and A_z-Mo_y-W_x-ca mixed oxides.

The catalysts in the form of fine powders soaked in the liquids as extracted from the reactor after the catalytic tests, were washed with toluene. Just before EXAFS analyses were performed, a portion was weighted and mixed with isopropyl alcohol for ultrasonication before the membrane was made. Kapton tape was used to cover the membrane.

2.7. Density functional theory calculations of the $Mo_{1-x}W_xS_2$ solid solution

A theoretical analysis of the cation distribution in $(Mo,W)S_2$ solid solutions was performed in

order to complement the EXAFS results, in particular to interpret the deviations of the experimental coordination functions from the ideal disorder behavior, as well as to assess the stability of the solid solution with respect to phase separation. The configurational spectrum of energies in a single-layer 4×4 supercell of $Mo_{1-x}W_xS_2$, for $x=i/16$ (i=0, …, 16) were calculated. Only the symmetrically different cation configurations, as found using the SOD code [40], needed to be calculated. The energy calculations were performed using density functional theory (DFT), as implemented in the VASP code [41, 42], using the PBE exchange correlation functional . The interaction between the valence electrons and the core was described with the projected augmented wave (PAW) method [43, 44], and the core levels up to 4*s* in Mo, 4*f* in W, and 2*p* in S were kept frozen in their atomic reference states. Both ionic positions and lattice parameters were relaxed for each configuration. Due to the large dimensions of the supercell, and the presence of a bandgap in the electronic structure, only the Γ point was used to sample the Brillouin zone for reciprocal space integrations.

2.8. Catalytic tests

The calcined mixed oxides were sulphided *in-situ* in a CS_2/n-hexadecane mixture in a batch Parr reactor. A careful sulphidation procedure was used, in order to avoid catalyst reduction before or after sulphidation. First, 1 g of catalyst was dried under nitrogen flow at 393 K for 2 h. A 200 cm^3 amount of a 5 vol % solution of CS_2 in n-hexadecane was added to the reactor. The amount of CS_2 added was calculated to be 5 times the stoichiometric one required to completely sulphide the unsupported mixed oxides. Next, under constant stirring at 400 rpm, the reactor was pressurised to 40 bar with hydrogen, heated to 503 K under constant pressure and kept at this temperature for 2h. It was then heated to 613 K under constant pressure and kept at this temperature for 16 h. Finally, it was cooled to 593 K and vented to atmospheric pressure, in order to remove the water and hydrogen sulphide formed during the sulphidation. Our XAFS data to be discussed subsequently showed that this protocol led to essentially

complete sulphidation of the catalysts. Once the sulphidation stage was finished, 5.75 g of DBT dissolved in 30 cm^3 of THN were added to the reactor. These amounts correspond to 280 ppmwt sulphur and 13 vol % THN in the reactor feed. Catalytic test conditions were then established (70 bar, 613 K, 600 rpm) and products evolution was followed by sampling small volumes of the reaction mixture for 6 h. Quantitative analysis of the reaction products was carried-out by gas chromatography in an Agilent 6890 instrument. The same chromatographic method and column (Agilent methylsiloxane 100 m X 250 µm X 0.50 µm) were used for identification of the products in an Agilent 6890 gas chromatograph equipped with a 5973A quadrupole mass selective detector.

The initial rates of conversion, R_0, for each reactant were determined from the slopes of percent conversion vs. time curves at time equals zero. Specific initial reaction rates, r_0 expressed in mol s^{-1} g_{cat}^{-1} were determined using the relation:

$$r_0 = \frac{R_0 n_0}{100 m_{cat}} \qquad (1)$$

where n_o and m_{cat} are the initial amount of reactant in the system and the catalyst mass, respectively. All sulphided samples were characterised after the catalytic tests.

3. Results

3.1. Characterisation of the oxide materials

3.1.1. X-ray diffraction and chemical analyses

The XRD patterns for all precursors are presented and briefly discussed in the supplementary Information (SI). In Fig.S1A, the XRD patterns for the Co_z-Mo_y-W_x-am precursors are shown. Peaks of the spectrum corresponding to the layered ϕ_y phase described by Levin et al.[45] (ICSD-165342) are present in all samples except in those with higher *X* values, that is,

$Co_{1.1}$-$Mo_{0.28}$-$W_{0.72}$-am and $Co_{1.2}$W-am. In the Ni_z-Mo_y-W_x-am systems (Fig. S1B), these peaks appear only in the $Ni_{1.6}$Mo-am material. Apart from those, broad peaks corresponding to an up to now unidentified phase are observed in the tungsten-rich materials of both series. This phase is also repeatedly reported in some patents on the production of Ni-Mo-W unsupported catalysts [5, 46].

A mentioned in topic 2.1, based on the decomposition temperatures observed in TGA, the Ni_z-Mo_y-W_x-am series was calcined at 673 K while the Co_z-Mo_y-W_x-am series was calcined at 623 K, in order to obtain the corresponding mixed oxides. Figs. S2A and S2B in the Supplementary Information show the respective XRD patterns. The reflections in the $Co_{1.1}$-Mo-ca and $Co_{1.2}$-W-ca oxides correspond, respectively, to those of β-$CoMoO_4$ and wolframite $CoWO_4$. For the trimetallic oxides, mixtures of these phases are seen to be present. The results are more complex in the case of the Ni_z-Mo_y-W_x-ca series. The pattern for $Ni_{1.6}$-Mo-ca is a mixture of those of α- and β-$NiMoO_4$ [31]. The XRD pattern for $Ni_{1.6}$-W-ca contains the same reflections observed in $Ni_{1.5}$-$Mo_{0.32}$-$W_{0.68}$-ca but appear less broadened. In none of the XRD patterns for the calcined oxides is there evidence for the presence of MoO_3, WO_3, NiO or CoO. The X-ray fluorescence analysis results for the mixed oxides are shown in Table 1.The expected and actual W/(W+Mo) and A/(W+Mo) molar ratios are reported.

The A/(Mo+W) ratios are larger than the 1:1 ratio used in the synthesis, especially in the case of nickel-containing materials. This is not totally unexpected as Levin has reported a 1.5 upper limit for the Ni:Mo ratio in ϕ_y phases [47], but some values in the nickel-containing series are considerably above this limit. Due to the fact that our Ni/(W+Mo) ratios were higher than 1, the presence of a small amount of an X-ray invisible Ni-containing phase, such as nickel oxide, may not be completely excluded. This was not the case of Co-containing precursors where the Co/(Mo+W) ratios are less than 1.5 and, as a consequence, the Co

excess could form, after calcination, a solid solution of Co simple oxide and β-$CoMoO_4$ phase [48], since the β-$CoMoO_4$ phase is stable at ambient condition. A brief discussion on the possibilities of the formed phases is made in the SI.

In the uncalcined oxides materials the XANES Mo-L_3 edges spectra (see Fig. S3A a) show the same XANES resonances as the Na_2MoO_4 pattern where Mo atoms are tetrahedrally coordinated. After calcination XANES spectra shown see Fig. S3A b) that great fraction of Mo atoms remain tetrahedrally coordinated. On the other hand W atoms in the trimetallic precursors are ochtaedrally coordinated as shown their XANES W-L_3 spectra (see Fig S3B).

In summary, the Ni/(Mo+W) ratio (and to a lesser extent the Co/(Mo+W) ratio too) is much higher than expected in the synthesis and the reason for this is likely to be related to the pH of the precursor synthesis solution, since Ni (Co) cations and protons compete for incorporation in the crystal structure of the ϕ_y phase. Thus, XANES spectra suggest that in the trimetallics Ni_z-Mo_y-W_x-am precursors, W atoms are not in the same crystal ϕ_y-phase positions as Mo atoms, otherwise, W atoms would be tetrahedrally coordinated. Further experimental investigation will be needed for a complete understanding of these issues and should be published elsewhere.

3.1.2. Textural properties and SEM

The textural properties of the A_z-Mo_y-W_x-ca mixed oxides are shown in Table 2. There are no pronounced differences among the surfaces areas between or within nickel-containing and cobalt-containing oxides. However, the three tungsten-richest oxides in the nickel series have larger pore volumes and pore diameters than the remaining oxides.

Figs. S4A and S4B of the SI shows the scanning electron micrograph (SEM) for $Ni_{1.7}$-$Mo_{0.50}$-$W_{0.50}$-am, $Co_{1.3}$-$Mo_{0.41}$-$W_{0.59}$-am precursors and the respective calcined oxides. We notice first that there is little change in particle morphology upon calcination. There is however a

pronounced difference in morphology between the nickel-containing and the cobalt-containing materials. The particles of the nickel-containing materials have a sponge-like texture, suggestive of the presence of large pores, where the texture of the cobalt-containing materials is more closed. This is consistent with the larger pore volume and average pore diameter of $Ni_{1.7}$-$Mo_{0.50}$-$W_{0.50}$-ca, as compared to $Co_{1.3}$-$Mo_{0.41}$-$W_{0.59}$-ca apparent in Table 2.

3.2 Characterisation of the sulphided materials

3.2.1. SEM, HR-(S)TEM and textural properties. The $Ni_{1.7}$-$Mo_{0.50}$-$W_{0.50}$ as compared to $Co_{1.3}$-$Mo_{0.41}$-$W_{0.59}$ materials were chosen for HR-(S)TEM and SEM characterisation. As compared to their respective precursors and mixed oxides (*cf.* Figures S4A and S4B), the morphologies of the $Ni_{1.7}$-$Mo_{0.50}$-$W_{0.50}$-s and $Co_{1.3}$-$Mo_{0.41}$-$W_{0.59}$-s materials are much smoother. Nevertheless, the morphology of the $Ni_{1.7}$-$Mo_{0.50}$-$W_{0.50}$-s sulphide after the catalytic test seems to have retained some of the roughness of the precursor calcined oxide. In the case of $Co_{1.3}$-$Mo_{0.41}$-$W_{0.59}$-s, considerable coalescence of the original mixed-oxide grains seems to have occurred during sulphidation and subsequent catalytic test (*cf.* Figures S5 from the SI).

Figs. 1a) and 1b) show representative high-resolution TEM images of $Ni_{1.7}$-$Mo_{0.50}$-$W_{0.50}$-s and $Co_{1.3}$-$Mo_{0.41}$-$W_{0.59}$-s, respectively. The presence of randomly distributed lamellar particles, typical of $Mo(W)S_2$, is clearly distinguished. The slabs are typically curved and individual particles are present with varying stacking degrees. The interlayer distance is ca. 6 Å, which is approximately the distance (6.15 Å) between (0 0 2) planes in the MoS_2 crystal structure. High-resolution images representative of the rest of the catalysts are shown in supplementary material (*cf.* Fig. S6A-D). The distribution for both $Ni_{1.7}$-$Mo_{0.50}$-$W_{0.50}$-s and $Co_{1.3}$-$Mo_{0.41}$-$W_{0.59}$-s catalysts slabs stacking degrees and average length (see the frequency count distribution in figure S7A and S7B) were obtained from measurements for about 120

particles (460 layers) in different images. The values are summarised in Table 3. Also, the statistics for the W-free catalysts are presented.

Both the average stacking number (ASN) and the average length determined from the HR-TEM measurements are larger for the sulphide particles in catalysts containing Co than in those containing Ni. The introduction of tungsten causes a decrease in ASN, both with Ni- and Co-containing sulphides. A number of long slabs are present which will represent a significant percentage of the Mo+W atoms present in the catalyst, i.e., the dispersion of the bulk catalysts under study is rather low. In the many HR-TEM images we have analysed we have not seen any Ni_xS_y or Co_xS_y crystallites, either segregated or surrounded by $Mo(W)S_2$ slabs, as has been reported in previous work, e.g. [2] and reference therein.

The elemental mapping in high-resolution mode for Co, Ni, Mo and W is presented in Fig. S8A. In the $Ni_{1.7}$-$Mo_{0.50}$-$W_{0.50}$-s catalyst (Fig. S8Ab) There is a homogeneous distribution of the elements. In $Co_{1.3}$-$Mo_{0.41}$-$W_{0.59}$-s catalysts (Fig. S8Aa) the same tendency is observed for the region studied, in that a homogeneous distribution is observed for W, Mo and S. However, in the STEM Co map, some islands are observed, which could be due to some CoS segregation in the sampled area. In Fig. S8B the sulphur elemental map is shown for both $Ni_{1.7}$-$Mo_{0.50}$-$W_{0.50}$-s and $Co_{1.3}$-$Mo_{0.41}$-$W_{0.59}$-s sulphides.

Table 4 shows the main textural properties of the sulphide catalysts, as determined by nitrogen physisorption. The corresponding nitrogen adsorption isotherms and pore size distribution curves are shown in Figs. S9 and S10. There was generally a decrease in BET surface area after sulphidation and catalytic test, but the effect was much more pronounced in the case of the cobalt series, so that, in general, the surfaces areas in the nickel series were larger than those in the cobalt series. There is an intrinsic decrease in BET surface area upon sulphidation as a result of an increase in the skeletal density of the material. However, the decrease in pore volumes was even larger than that of surface areas, and was accompanied by

a pronounced decrease in average pore diameter. The small BET areas in the Co-series sulphides as compared with the Ni-series correspond to their higher large average length and average stacking number in the HR-TEM analysis. Oxidation of the sulphides prior to BET analysis is very unlikely, due to the sulphide recovery procedure used (*c.f.* experimental section 2.4).

3.2.2. X-Ray Absorption of sulphides

3.2.2a. XANES. The XANES region at Co K- , Ni K-, Mo K- and W L_3–edges regions of the X-ray absorption spectra for the Co_z-Mo_y-W_x-s and Ni_z-Mo_y-W_x-s series are shown in Figs. S11A, S11B, S12A-B and S13A-B of the SI, respectively. It should be noted that, due to the careful procedure used during the sulphidation process (*c.f.* section 2.8) the metals were completely sulphided, as evidenced by the XANES spectra taken at W L_3-, Mo K- and Ni K- or Co-K edges; see the explanations in the SI.

3.2.2b. EXAFS Ni K- and Co K-edges

The extracted EXAFS oscillations and the k^3-weighted FT from Co and Ni K-edges X-rays absorption spectra of A_z-Mo_y-W_x-s catalysts of both series are shown in Fig. S14A and S14B of the SI. Tables S1A and S1B in the SI show the parameters obtained from the simulation for the nickel and cobalt series, respectively, from EXAFS simulations. The A (Ni or Co) second-sphere coordination number (A-A interaction) shown in Tables S1 equals approximately 2 for most of the catalysts, implying that A atoms would be present in small sulphide clusters. An hypothesis is that the A is present as an atomically dispersed species, such as in the so-called AMo(W)S phase [6], coexisting with large A_xS_y crystallites as reported recently for Co-promoted unsupported systems [19]. If a large portion of the nickel was atomically dispersed, a peak due to the NiMoS species would be expected at 2.85 Å in the Fourier-transformed Ni K-edge EXAFS spectra of the catalysts [49-51]. The absence of

this peak, however, does not necessarily imply that the NiMo(W)S phase is absent from our catalysts, since it may have remained undetected because the corresponding nickel signal was overwhelmed by a more abundant Ni_3S_2-like phase.

The low A-A (A=Ni,Co) coordination numbers confirm that the A_xS_y sulphides have not a crystalline structure. Besides, analyzing the Crystallographic Information File of the A_xS_y used in the EXAFS simulation, the A-S coordination number is as low as 4. [30, 52]. These low A-S and A-A coordination numbers have been discussed in previous work, e.g. [53]

3.2.2c. EXAFS Mo K- and W L_3-edges. Figs. 2a and 2b show the Mo-K the k^3-weighted FT spectrum for molybdenum-containing catalysts, both of the Ni and the Co series. The same symbols are used for the same nominal W:Mo ratio in both series. Two peaks are distinguished in each series, the first one corresponding to the Mo-S interaction and the second corresponding to the combined Mo-Mo and Mo-W interactions. In both cases the second shell Mo-Mo(W) intensity decreases markedly as the W content increases. This is due to destructive interference between the molybdenum-emitted outgoing electron wave and the ones backscattered by tungsten atoms located at the second coordination shell of the emitting molybdenum atom. This effect is reported for intralayer $Mo_{1-x}W_xS_2$ solid solutions obtained from thiosalts [12]. The k^3-weighted FT for the EXAFS oscillations extracted from the W L_3-edge spectra from both Ni- and Co-series sulphides, are shown in Fig. S15 from the SI. Given the fact that for each trimetallic sulphide, both Mo K and W L_3-edge EXAFS have been experimentally obtained, it is reasonable to do a simultaneous fitting of the R-space distribution functions of both edges, in order to decrease the number of independent parameters used in the simulation. Effectively, the constraints should be imposed in the second coordination shell from which both spectra have common information. In this work the S_0^2 values for the fitting of the spectra in the Mo K- and W L_3-edges were the ones

obtained from the fitting of the spectra of, respectively, the MoS_2 and WS_2 standards, in order to minimise the error in coordination number (*CN*) determination, as suggested by Kelly and Ravel [54].

The total second shell coordination number of either molybdenum or tungsten was taken as 6.0, assuming that the fraction of incompletely coordinated atoms is negligible, which is reasonable, since all materials are bulk sulphides. Besides, if the formation of a binary sulphide $Mo_{1-x}W_xS_2$ is considered, four second shell average *CN*s need to be considered, namely Z_{MoMo}, Z_{MoW}, Z_{WMo} and Z_{WW}, where, in Z_{A-B}, A is the central atom and B is an atom in the second coordination shell. It can be demonstrated (*cf.* topic S1.1 in the SI) that only one of these is an independent variable that needs to be determined from the spectral fitting. All the others may be determined from this one, considering that the total *CN* of any metal atom is 6, taking into account the *x* value in the formula of the mixed sulphide, determined by X-ray fluorescence analysis, and assuming that Mo and W are randomly distributed in the slabs.

The crystal structure of MoS_2 (ICSD-601647) was used in Artemis code [55] for the EXAFS path generation in the Mo K-edge with a second shell shared by Mo atoms and W atoms. For the W L_3-edge path generation, the WS_2 (ICSD- 84181) was used instead, also with a second shell shared by W and Mo atoms. Additionally, the Mo-W Debye-Waller factors and interatomic distances were the same for the simultaneous fitting of both absorption edges, since these parameters should be invariable independent of the absorber atom, W or Mo.

In Table 5 the results for parameters determined from the EXAFS simultaneous fitting are shown for the second shell of trimetallic sulphides. The third column in the table (x_{AB}) shows the fraction of atom B in the second coordination shell of atom A. The results for all catalysts (including the first shell) and for the MoS_2 and WS_2 commercial pattern are reported in Table S2A and S2B in the SI.

Comparison of the x_{AB} values presented in Table 5 for the Ni series with the tungsten molar percentages shown in Table 1, indicates that, within the error of this parameter, the fraction of a given element in the second coordination shell of a given central element cannot be distinguished from the overall composition of the sulphides. This suggests that a random distribution of Mo and W actually exists within the sulphide slabs of the Ni series. In the case of the Co-series sulphides, the x_{AB} ratios are also close to the full disorder limit, but more significant deviations are obtained, in particular for $Co_{1.1}$-$Mo_{0.28}$-$W_{0.72}$-s, where a much smaller fraction of Mo around Mo than expected was obtained, while the error in the estimation of the parameter was very small. The $Co_{1.1}$-$Mo_{0.28}$-$W_{0.72}$-s sulphide has an exceptionally low intensity of the second shell in the Mo K-edge spectrum due to the high W content, so for its simulation the Mo-Mo(W) distance and Debye-Waller factor were fixed to that of the W-W second shell in the WS_2 pattern fitting, thus the small error bar. As an example, the simulations of radial distribution functions for $Ni_{1.7}$-$Mo_{0.50}$-$W_{0.50}$-s and $Co_{1.3}$-$Mo_{0.41}$-$W_{0.59}$-s catalysts are shown in Figure 3. For the rest of the trimetallic catalysts, the same fittings are shown in Figure S16 in the SI.

From the EXAFS simulations it may be concluded that the trimetallic sulphides used as catalysts form intralayer solid solutions. From Table 5, the Debye-Waller factor values are always larger for the Mo-W interaction that for Mo-Mo or W-W pairwise interactions, which also reflects the contribution to static disorder due to the presence of both cations located in equivalent positions of the same slabs. For simultaneous (R-space) fitting of W L_3- and Mo K- edges EXAFS we have not imposed any restrained values for the M-M (M = Mo or/and W) distance in the second shell for the trimetallic sulphides. The errors in the M-M distances reported for the $Co_{1.2}$-$Mo_{0.69}$-$W_{0.31}$-s and $Co_{1.3}$-$Mo_{0.41}$-$W_{0.59}$-s samples are higher maybe due to a higher static disorder in these samples, which is also reflected in the higher Debye-Waller values. The model proposed is good if we take in to account the *R*-factor values

obtained for the fitting and that the XRF composition was imposed.

3.3. DFT calculations of the $Mo_{1-x}W_xS_2$ solid solution

Figure 4a shows the mixing energies for all the total 843 configurations generated in the 4x4 supercell (*cf.* 2.7), as a function of *x*. These mixing energies represent the energetic cost (normalised per formula unit) of creating the mixed sulphide in a particular configuration, from the corresponding amounts of pure MoS_2 and WS_2. This figure demonstrates that the mixed sulphide with any composition $Mo_{1-x}W_xS_2$ is energetically favoured with respect to the pure sulphides. The mixing is only slightly exothermic, but configurational entropy contributions, not shown in this figure, will further stabilise the formation of the solid solution. The thermodynamic stability of the solid solution is consistent with our experimental observation of atomically homogeneous mixed sulphides.

Our DFT results show that the most stable configuration for each composition is always one where the distribution of W and Mo is the most homogeneous. Conversely, the least stable configuration is always one where the cations of the same species cluster together. For example, for the supercell with composition $Mo_{12}W_4S_{32}$, the energies of the configurations increase linearly with the nearest-neighbour coordination number Z_{WW} (figure 4b). Note that the parameter Z_{WW} fully characterises the nearest-neighbour coordination environment in the mixed solids, as the other coordination numbers (Z_{MoMo}, Z_{MoW}, Z_{WMo}) are determined by the value of $Z_{WW.}$ In the lowest-energy $Mo_{12}W_4S_{32}$ configuration, Z_{WW}=0 and the W atoms are as far as possible from each other.

These results can help us elaborate a possible interpretation for the deviations of the experimental coordination numbers from the expected values based on the assumption of full disorder. In Fig. 5 we have plotted the Z_{WW} determined by EXAFS for the trimetallic sulphides, in comparison with the expected values of Z_{WW} for the fully disordered case

(corresponding to the diagonal straight line function: 6*x*). We also plot the equilibrium Z_{WW} values obtained from the weighted average of the DFT energies in the configurational spectrum using Boltzmann factor weights [40, 56-58] at room temperature. These equilibrium values of Z_{WW} are below what is expected for the fully random distribution, due to the thermodynamic tendency to partial ordering with maximum homogeneity. In the EXAFS results, there is a tendency for the nickel series to be closer to the fully random case, whereas the cobalt series is closer to the thermodynamic preference, i.e., it tends to have lower Z_{WW} values. However, the errors bars for the experimental coordination numbers are large, so this interpretation would require further investigation. The slightly different cation distribution in the two series of sulphides, if confirmed, may be related to the different nature of the oxide phases from which they formed.

3.4. Catalytic tests

The curves for DBT and THN (tetralin) conversion *vs.* time for both the Ni and Co sulphide series are shown in Fig. 6. Two families of curves are distinguished depending of the promoter used. For both reactions, the initial rates of DBT and THN conversions are higher for the Ni series than those for the Co series sulphides. It is also observed that there is an acceleration of the hydrogenation reaction, indicated by an upward curvature of THN conversion *vs.* time curve. This is likely due to a stronger inhibition of THN hydrogenation by DBT than by the HDS products, including hydrogen sulphide.

Figs. 7 and 8 show examples of product yield *vs.* conversion curves, in the HDS of DBT and in THN hydrogenation for $Ni_{1.7}$-$Mo_{0.50}$-$W_{0.50}$-s and $Co_{1.3}$-$Mo_{0.41}$-$W_{0.59}$-s catalysts, respectively. The rest of the curves are shown in the SI, Figures S17A-D. In both catalysts series the points corresponding to THN hydrogenation products follow quite accurately straight lines. The curve for biphenyl (BPH) formation has a slight downward curvature,

while that for cyclohexylbenzene (CHB) formation has an upward curvature, indicating the occurrence of BPH hydrogenation to CHB.

For the purpose of studying catalyst selectivity, a previously reported network of irreversible pseudo-first order reactions was assumed for the HDS of DBT (Scheme 1), noticing that the reaction was carried-out under constant hydrogen pressure. The reader is referred to reference [31], where the equations used to determine the kinetic parameters for the model described below are shown and justified.

In Scheme 1, DDS, HYD and BPH represent, respectively, the *direct desulphurisation route*, that leads directly from DBT to BPH, the *prehydrogenation route*, that leads from DBT to CHB, and BPH *hydrogenation*, that leads from BPH to CHB. The results obtained for k_{DDS}, k_{HYD} and k_{HBP} values are reported in Table 6. The lines in Fig.7a and Fig.8a represent the best fit with this simple model. Similar curves for the rest of the catalysts studied are shown in Figure S17 in the SI.

In tetralin hydrogenation, straight lines were obtained when the yield of each product was plotted against tetralin conversion, with both series of unsupported sulphides. Therefore, no evidence exists for interconversion between the isomeric products *cis*- and *trans*- decalin. In this case, selectivity was analysed simply in terms of the ratio of initial rates of formation of both products.

The activity and selectivity results of catalytic tests for simultaneous HDS of DBT and HDA of THN are shown in Table 6 for both Ni and Co promoted unsupported catalysts. For comparison, the results for an alumina-supported NiMo catalyst with a 1:1 nickel to molybdenum ratio, whose characterisation was already reported [31, 36], are also shown.

The r_{HDS} and r_{HDA} activity results shown in Table 6 are reported per catalyst total (W+Mo) metal content. On this basis, the unsupported catalysts belonging to both the nickel and the

cobalt series have DBT HDS activities that are one order of magnitude lower than the supported $NiMo/Al_2O_3$ catalyst, due to the much higher dispersion of the sulphide in the former case. The same order of magnitude is observed when activities are reported on a weight basis (*c.f.* Tables S3 in the SI). However, if the activity was reported per catalyst volume, as is commonly done for commercial catalyst, the bulk sulphides would certainly be considerably more active than the supported one, because the bulk sulphide materials are much denser than the supported ones.

Although it could be expected, as observed, that the nickel-containing sulphides were more active than the cobalt-containing ones in aromatic hydrocarbon hydrogenation, they were also more active in DBT HDS, although in this case the difference was much smaller. The difference does not disappear when activities per unit surface area are considered. On the pseudo-TOF basis, the $Ni_{1.5}$-$Mo_{0.32}$-$W_{0.68}$-s catalyst has a greater activity in the THN HDA than the rest of unsupported catalysts and it has a good performance in the DBT HDS reaction.

An important point that emerges from the data in Table 6 is that, despite the fact that our characterisation results demonstrate that molybdenum and tungsten are intimately mixed in the trimetallic sulphides, no synergetic effects are observed between the two elements, for the model feed used here. Neither activity (r_{HDS} and r_{HDA}) nor selectivity parameters present any significant maxima or minima for the trimetallic catalysts with respect to the bimetallic ones.

Due to the fact that the catalysts were sulphided in-situ in the liquid phase and the characterisation of the sulphides was performed with the material recovered from the catalytic tests, we considered that characterisation aiming at measuring active site density by common chemisorption techniques would not be representative of the catalysts in working conditions. Therefore, selectivity parameters are more interesting to correlate with catalyst composition.

In the nickel series, when tungsten is introduced in the catalyst composition, perhaps surprisingly the k_{HYD}/k_{DDS} ratio is hardly affected, while the r_{HDA}/r_{HDS} ratio increases and the *cis-/trans-* decalin ratio decreases with increasing tungsten content. The fact that there is an increase in selectivity for *trans*-decalin formation when the r_{HDA}/r_{HDS} ratio increases, indicates that tungsten addition improved the hydrogenation activity mainly of the sites involved in *trans*-decalin formation. This could also explain why the k_{HYD}/k_{DDS} is essentially insensitive to the tungsten content: according to a model previously proposed by us [31], the sites involved in *trans*-decalin formation are the same responsible for the DDS route in DBT HDS, not the ones involved in the HYD route. Therefore, an increase in the activity for hydrogenation of the DBT ring due to tungsten addition favouring the HYD route, is accompanied by an increase in activity for DBT HDS via the DDS route.

The selectivity for the HYD route in HDS (direct CHB formation) was much higher with the bulk Ni promoted catalysts than with the Co-promoted unsupported ones, which were clearly more selective for the DDS route (BPH formation). This is in agreement with what is known in the literature [59, 60]. It should be said that since the DBT conversion achieved was smaller in the case of the bulk sulphides containing Co and (as in the case of $NiMo/Al_2O_3$ catalyst prepared in our lab) the k_{BPH}/k_{DDS} ratio was not reported in Table 6 since the reliability of this value in not guaranteed with the kinetic model employed.

Consistently with the increase in r_{HDA}/r_{HDS} with increasing tungsten content, the activity for biphenyl hydrogenation to cyclohexylbenzene relative to HDS (k_{BPH}/k_{DDS}) increases in the same direction. Differently from the nickel series, the selectivity parameters of cobalt-containing catalysts changed very little with the Mo/W proportion. The *cis-/trans-* decalin ratio was constant and similar to that of the bimetallic NiMo sulphide, i.e., considerably larger than that of the $NiMo/Al_2O_3$ catalyst. Also the k_{HYD}/k_{DDS} ratios, although smaller than those of the nickel series, were larger than the ones of the supported NiMo catalyst.

Finally, it is interesting that, despite the fact that the CoW combination is generally considered to be the worst of the four possible ones in hydrotreating catalysis, the unsupported CoW sulphide had a HDS activity similar to that of a CoMo unsupported sulphide with similar total surface area, both in DBT HDS and THN hydrogenation.

4. Conclusions

Bimetallic (Ni-Mo and Co-Mo) and trimetallic (Ni-Mo-W and Co-Mo-W) unsupported sulphides were prepared from mixed oxide precursors in which W atoms were not incorporated in the ϕ_y lamellar phase oxide precursor by the syntheses condition used.

Regardless of the W/Mo ratio in the mixed-oxide precursor, the EXAFS analysis of the corresponding bulk sulphides obtained by liquid sulphidation showed the presence of Mo-W pairs connected by sulphur ions, indicating the formation of intralayer Mo1-xWxS2 solid solutions. The Mo/W crystallographic sites in the sulphides are occupied randomly by any of these cations, which leads to a slightly negative energy of mixing of the solid solution as demonstrated by DFT calculations. This is in agreement with the homogeneous cation distributions observed by STEM. EXAFS also shows that A (Ni or Co) sulphide entities are forming part of small A_xS_y particles with a reduced A-A coordination number.

With the model feed and testing conditions used in this work, no synergetic effect between molybdenum and tungsten could be observed, either in terms of activity or selectivity. The main factor affecting activity and selectivity was the nature of the promoters, not of the group 6 elements; nickel-containing catalysts were more active than the cobalt-containing ones, especially in tetralin hydrogenation. With increasing tungsten proportion, the selectivity of the nickel containing catalysts for the hydrogenation of aromatic hydrocarbons relative to DBT HDS increased, but the relative contribution of the two competing routes for the HDS reaction (direct desulphurisation and previous ring hydrogenation) was rather insensitive to

the proportion between the group 6 elements. In the series of cobalt-containing catalysts, both activities and selectivities were essentially insensitive to the composition of the group 6 sulphide phase.

Despite the fact that cobalt-containing catalysts are less hydrogenating than nickel-containing ones, the preference for the previous ring hydrogenation route over the DDS route of the unsupported cobalt-containing catalysts in DBT HDS was higher than that of an alumina-supported NiMo catalyst, highlighting the influence of support interactions on the performance of this class of catalyst

Acknowledgments

The authors would like to thanks PETROBRAS and CNPq (for financial support and Laboratório Nacional de Luz Síncrotron (LNLS) for project XAS XAFS1- 9136, XAFS2 10161, D10B-XPD 9914 and Laboratório Nacional de Nanotecnología LNANO for HR-TEM 10300 and 11528 approvals. NUCAT (COPPE/UFRJ - Brazil) for XRF, Laboratório Multiusuário (IQ/UFRJ - Brazil) for XRD. ACFJ thanks CNPq for a research scholarship. YLF thanks CAPES-PAEX program for funding his attendance to MACS IV event. For the theoretical work we used ARCHER, the UK's national high-performance computing service, via the UK's HPC Materials Chemistry Consortium, which is funded by EPSRC (EP/L000202).

Appendix A. Supplementary data

Supplementary data associated with this article can be found, in the online version, at XXX.

Figures and captions

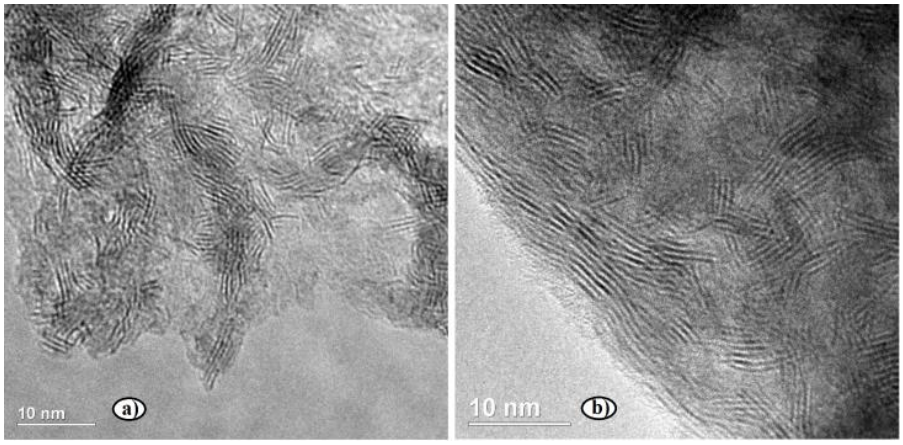

Figure 1. HR-TEM images for a) $Ni_{1.7}$-$Mo_{0.50}$-$W_{0.50}$-s and b) $Co_{1.3}$-$Mo_{0.41}$-$W_{0.59}$-s.

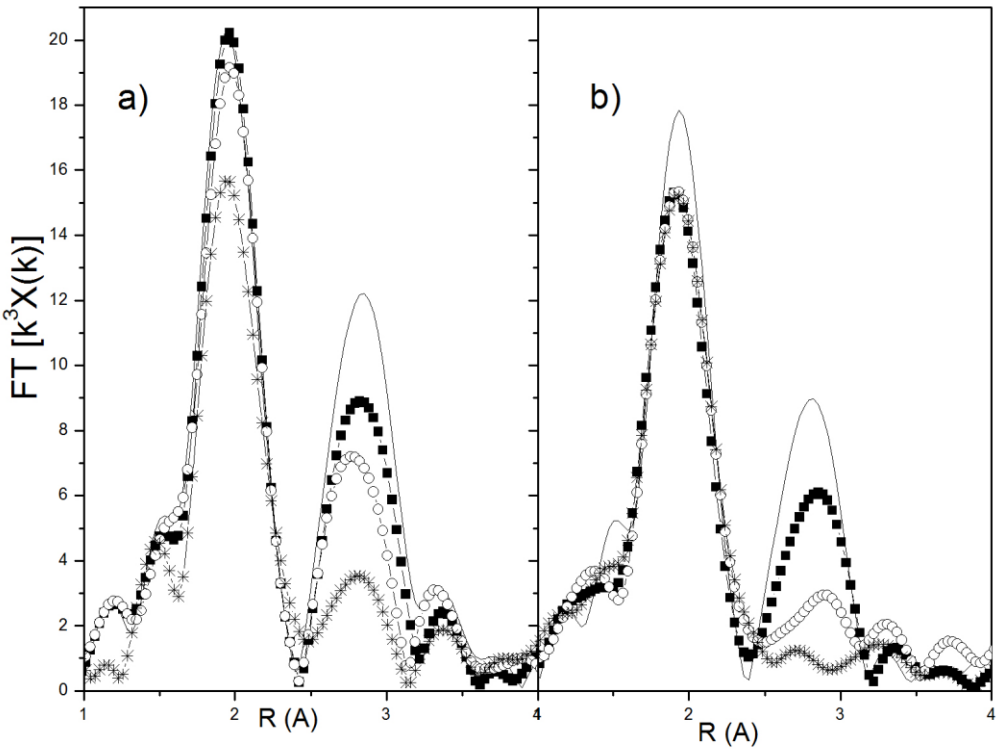

m

Figure 2. Mo K-edge k^3-weighted FT from EXAFS oscillation for **a)** the Ni promoted catalysts containing Mo and **b)** for the Co-promoted catalysts containing Mo. Symbols are: solid line for $Ni_{1.6}$-Mo-s and $Co_{1.1}$-Mo-s; ■ for $Ni_{1.9}$-$Mo_{0.62}$-$W_{0.38}$-s and $Co_{1.2}$-$Mo_{0.69}$-$W_{0.31}$-s; ○ for $Ni_{1.7}$-$Mo_{0.50}$-$W_{0.50}$-s and $Co_{1.3}$-$Mo_{0.41}$-$W_{0.59}$-s ; ⁎ for $Ni_{1.5}$-$Mo_{0.32}$-$W_{0.68}$-s and $Co_{1.1}$-$Mo_{0.28}$-$W_{0.72}$-s .

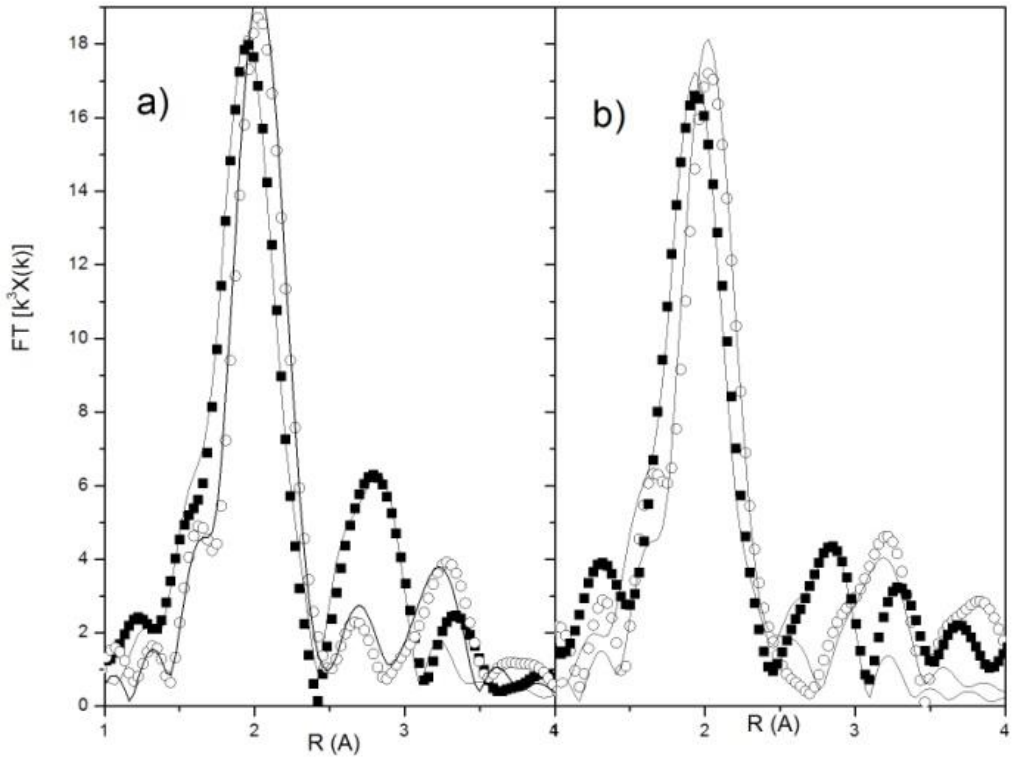

Figure 3. R-space Mo K and W L_3-edges simultaneous EXAFS simulation for **a)** $Ni_{1.7}$-$Mo_{0.50}$-$W_{0.50}$-s and **b)** $Co_{1.3}$-$Mo_{0.41}$-$W_{0.59}$--s. Symbols are: Solid lines are fitting lines; ■ Mo K-edge and ○ W L_3-edge k^3-weighted FT.

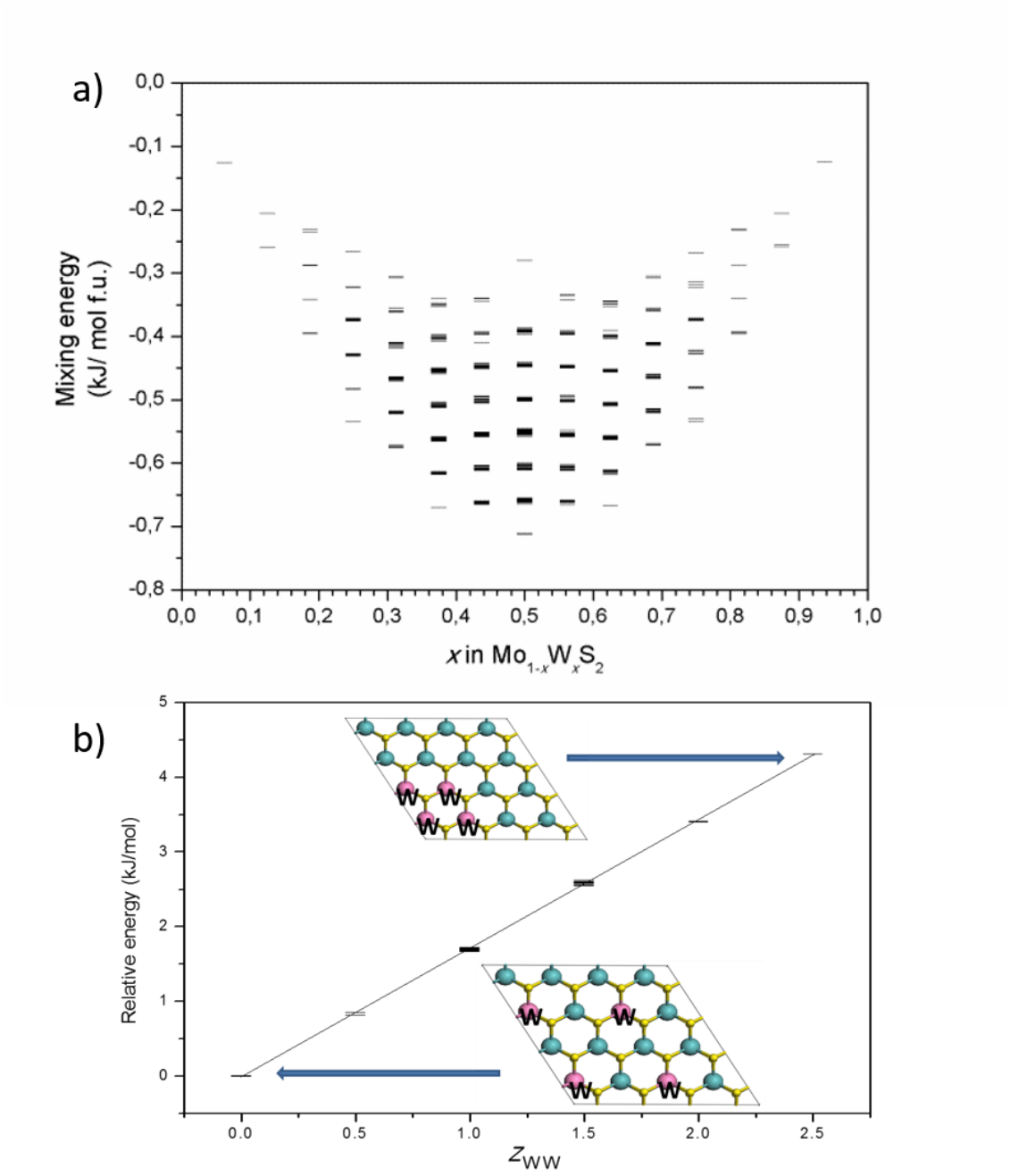

Figure 4. a) Mixing energy *vs x* in the different $Mo_{1-x}W_xS_2$ configurations as obtained from DFT calculations. b) Relative energies of the configurations with composition $Mo_{12}W_4S_{32}$ versus the average W-W coordination number in the configurations.

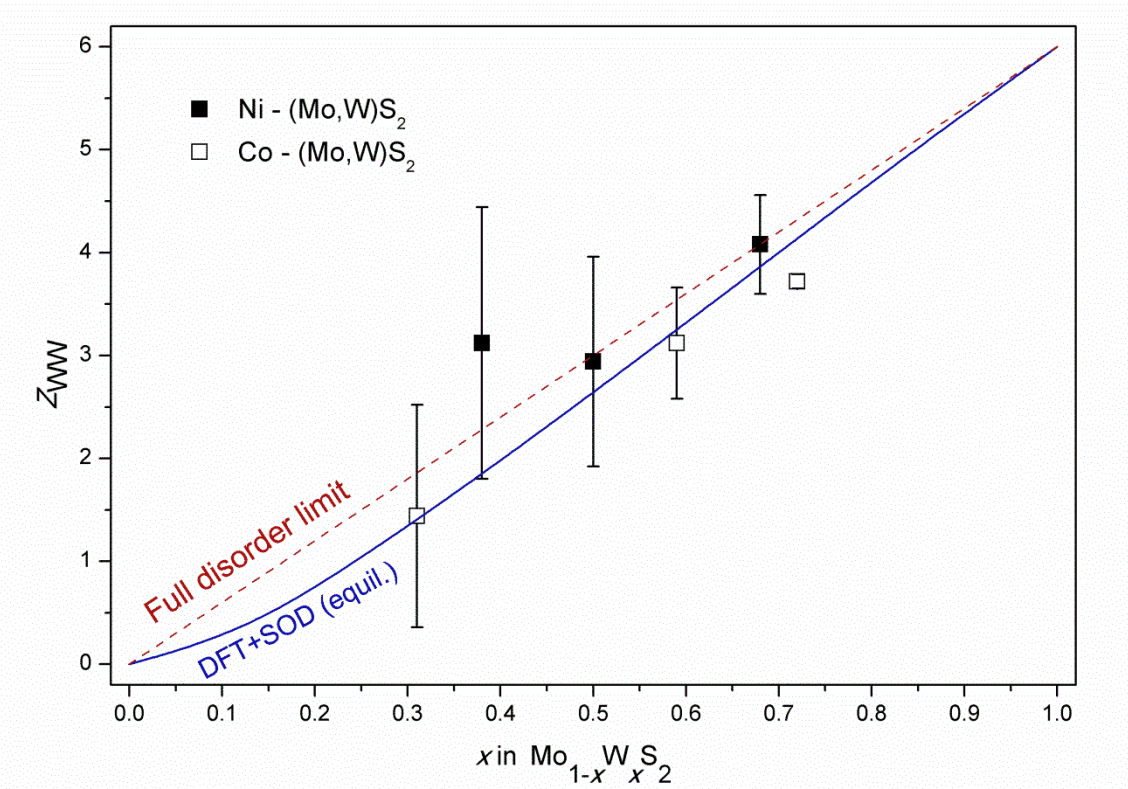

Figure 5. Z_{WW} coordination number *vs* composition in the $Mo_{1-x}W_xS_2$ compounds. Symbols are: red dashed line for the fully disordered case $Z_{WW}=6x$; EXAFS-determined Z_{WW} for sulphides of the Ni-series (solid squares) and the Co-series (open squares) of sulphides, and their error bars; solid blue line for the 'equilibrium' Z_{WW} values determined by configurational average of the DFT results.

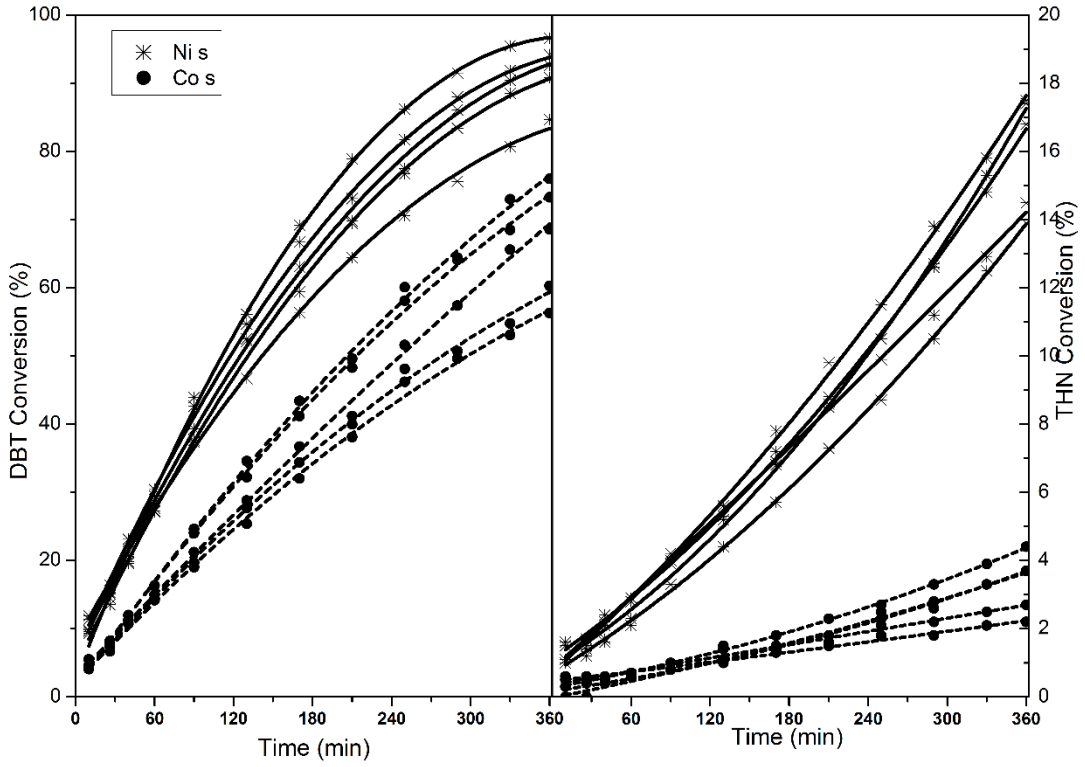

Figure 6. Conversion *vs* time for **a)** DBT HDS and **b)** HDA THN. Symbols are: solid lines and * for Ni_z-Mo_y-W_x-s series; dashed lines and • for Co_z-Mo_y-W_x-s series.

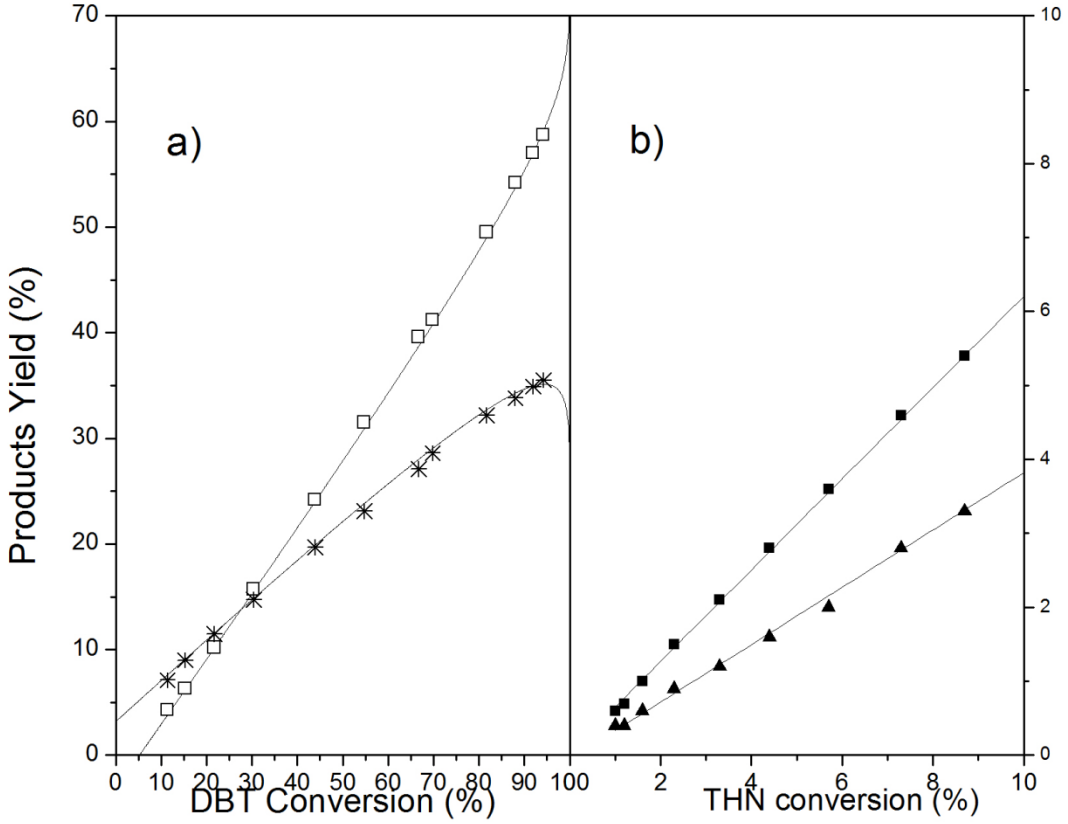

Figure 7. Products yield *vs* reactant conversion for $Ni_{1.7}$-$Mo_{0.50}$-$W_{0.50}$-s bulk sulphide catalyst. **a)** □ CHB and * BPH and first order fit (solid lines). **b)** ♦ *cis*-decalin and ▲*trans*-decalin and zero order fit (solid lines).

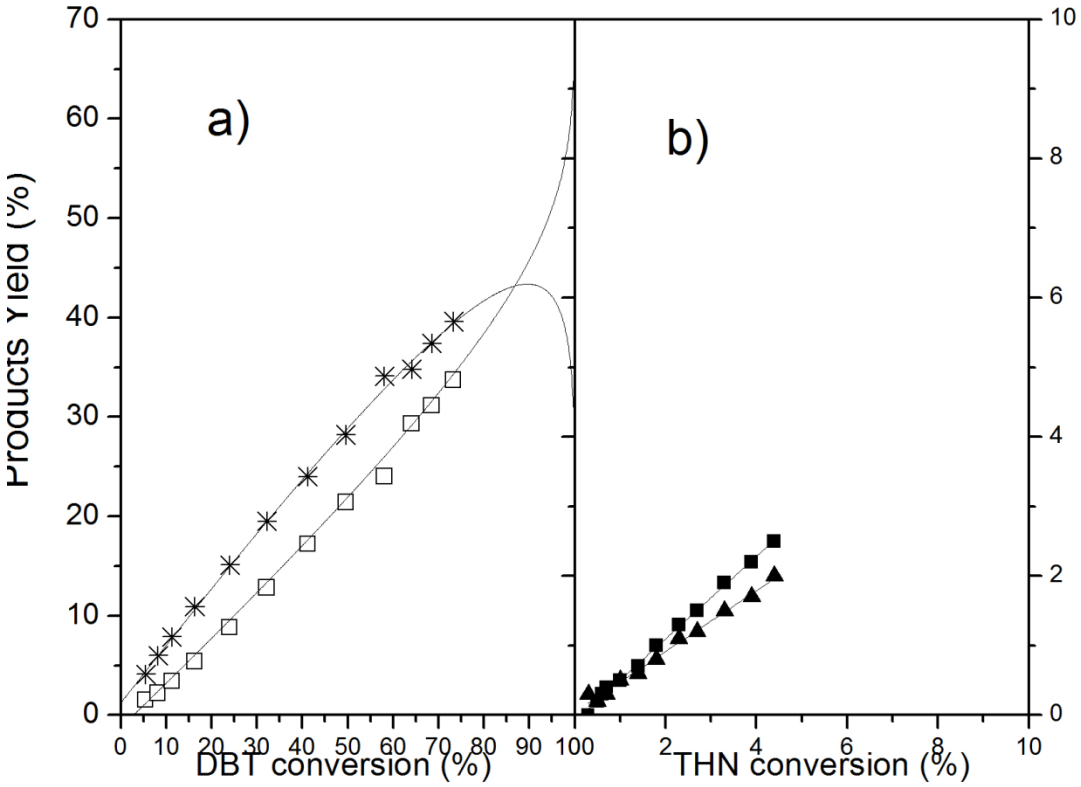

Figure 8. Products yield *vs* reactant conversion for $Co_{1.3}$-$Mo_{0.41}$-$W_{0.59}$-s bulk sulphide catalyst. **a)** □ CHB and * BPH and first order fit (solid lines). **b)** ♦ *cis*-decalin and ▲*trans*-decalin and zero order fit (solid lines).

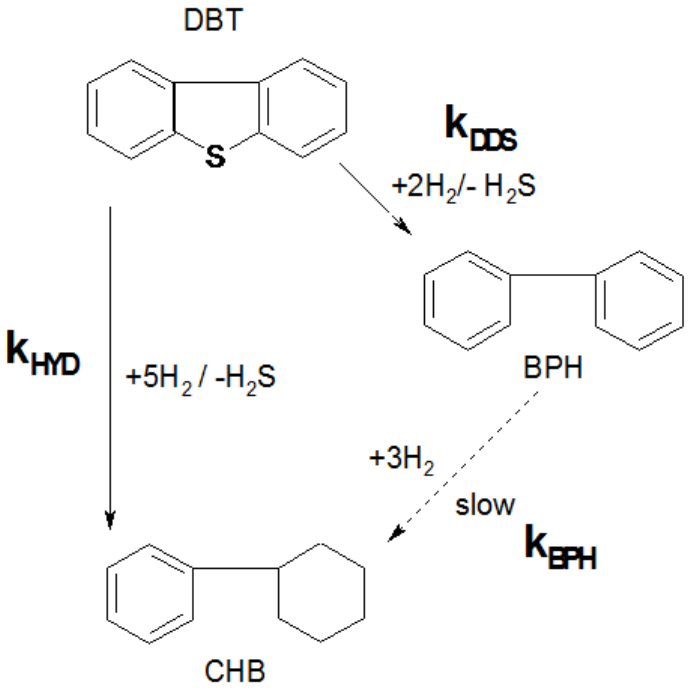

Scheme 1. Kinetic network proposed for HDS of DBT

TABLES

Table 1. Labels for mixed-oxide samples and compositions from X-ray fluorescence.

Mixed Oxides (A_z-Mo_y-W_x-ca)[a]	W/(W+Mo)[b] (synthesis)	A/(W+Mo)[b] (synthesis)	W/(W+Mo)[b] (actual)	A/(W+Mo)[b] (actual)
$Ni_{1.6}$-Mo-ca	0	1.0	0	1.6
$Ni_{1.9}$-$Mo_{0.62}$-$W_{0.38}$-ca	0.333	1.0	0.379	1.9
$Ni_{1.7}$-$Mo_{0.50}$-$W_{0.50}$-ca	0.5	1.0	0.502	1.7
$Ni_{1.5}$-$Mo_{0.32}$-$W_{0.68}$-ca	0.667	1.0	0.683	1.5
$Ni_{1.6}$-W-ca	1	1.0	1	1.6
$Co_{1.1}$-Mo-ca	0	1.0	0	1.1
$Co_{1.2}$-$Mo_{0.69}$-$W_{0.31}$-ca	0.333	1.0	0.312	1.2
$Co_{1.3}$-$Mo_{0.41}$-$W_{0.59}$-ca	0.5	1.0	0.589	1.3
$Co_{1.1}$-$Mo_{0.28}$-$W_{0.72}$-ca	0.667	1.0	0.724	1.1
$Co_{1.2}$-W-ca	1	1.0	1	1.2

[a] z=A/(W+Mo), X= W/(W+Mo), Y=1-X; [b]molar ratios; A=(Ni, Co)

Table 2**.** Textural properties for the A_z-Mo_y-W_x-ca mixed oxides

Mixed Oxides	BET area (m^2g^{-1})	Pore volume (cm^3g^{-1})	[a]APD (nm)
$Ni_{1.6}$-Mo-ca	30	0.05	7
$Ni_{1.9}$-$Mo_{0.62}$-$W_{0.38}$-ca	43	0.11	10
$Ni_{1.7}$-$Mo_{0.50}$-$W_{0.50}$-ca	40	0.23	23
$Ni_{1.5}$-$Mo_{0.32}$-$W_{0.68}$-ca	34	0.21	25
$Ni_{1.6}$-W- ca	68	0.25	15
$Co_{1.1}$-Mo-ca	49	0.12	10
$Co_{1.2}$-$Mo_{0.69}$-$W_{0.31}$-ca	59	0.16	11
$Co_{1.3}$-$Mo_{0.41}$-$W_{0.59}$-ca	66	0.16	10
$Co_{1.1}$-$Mo_{0.28}$-$W_{0.72}$-ca	49	0.14	11
$Co_{1.2}$-W-ca	45	0.13	12

[a]Average pore diameter (4V/A)

Table 3. Distribution of slabs stacking degrees and average length from measurements in the HR-TEM images of some catalysts

Catalyst	L (nm)[a]	ASN[b]
$Ni_{1.7}$-$Mo_{0.50}$-$W_{0.50}$-s	34	3.3
$Ni_{1.6}$-Mo-s	29	3.9
$Co_{1.3}$-$Mo_{0.41}$-$W_{0.59}$-s	42	3.9
$Co_{1.1}$-Mo-s	41	4.9

[a]Average length. [b]Average stacking number.

Table 4**.** Textural properties for the A_z-Mo_y-W_x-s sulphides

Sulphides	BET area (m^2g^{-1})	Pore volume (cm^3g^{-1})	APD (nm)[a]
$Ni_{1.6}$-Mo-s	35	0.05	5.7
$Ni_{1.9}$-$Mo_{0.62}$-$W_{0.38}$-s	33	0.08	9.7
$Ni_{1.7}$-$Mo_{0.50}$-$W_{0.50}$-s	24	0.05	8.3
$Ni_{1.5}$-$Mo_{0.32}$-$W_{0.68}$-s	26	0.06	9.2
$Ni_{1.6}$-W- s	40	0.05	5.0
$Co_{1.1}$-Mo-s	15	0.02	5.3
$Co_{1.2}$-$Mo_{0.69}$-$W_{0.31}$-s	24	0.07	12.0
$Co_{1.3}$-$Mo_{0.41}$-$W_{0.59}$-s	17	0.03	7.1
$Co_{1.1}$-$Mo_{0.28}$-$W_{0.72}$-s	28	0.05	7.1
$Co_{1.2}$-W-s	20	0.03	6.0

[a]Average pore diameter (4V/A)

Table 5. EXAFS parameters from simultaneous Mo K- and W L_3 –edges simulation for A_z-Mo_y-W_x-s trimetallic sulphides

Catalyst	2nd Shell	x_{AB}	*R(*Å)	σ^2(Å^2).10^3	*R-factor*(%) [Mo-K; W-L_3]
$Ni_{1.9}$-$Mo_{0.62}$-$W_{0.38}$-s	Mo-Mo	0.7±0.1	3.16±0.02	5.5±1.4	
	Mo-W	0.3±0.1	3.17±0.02	9.1±2.7	[1.3; 1.1]
	W-Mo	0.5±0.2	3.17±0.02	9.1±2.7	
	W-W	0.5±0.2	3.16±0.01	7.2±1.4	
$Ni_{1.7}$-$Mo_{0.50}$-$W_{0.50}$-s	Mo-Mo	0.5±0.2	3.16±0.01	4.9±1.6	
	Mo-W	0.5±0.2	3.19±0.02	10.5±3.9	[0.8; 1.3]
	W-Mo	0.5±0.2	3.19±0.02	10.5±3.9	
	W-W	0.5±0.2	3.17±0.02	6.6±2.8	
$Ni_{1.5}$-$Mo_{0.32}$-$W_{0.68}$- s	Mo-Mo	0.3±0.1	3.15±0.01	5.5±1.0	
	Mo-W	0.7±0.1	3.16±0.01	9.2±2.4	[3.7; 1.2]
	W-Mo	0.3±0.1	3.16±0.01	9.2±2.4	
	W-W	0.7±0.1	3.16±0.01	7.1±0.5	
$Co_{1.2}$-$Mo_{0.69}$-$W_{0.31}$-s	Mo-Mo	0.65±0.08	3.15±0.01	6.3±1.3	
	Mo-W	0.35±0.08	3.20±0.04	11.1±6.5	[2.9; 1.6]
	W-Mo	0.8±0.2	3.20±0.04	11.1±6.5	
	W-W	0.2±0.2	3.20±0.04	4.7±3.5	
$Co_{1.3}$-$Mo_{0.41}$-$W_{0.59}$-s	Mo-Mo	0.3±0.1	3.16±0.03	6.8±2.9	
	Mo-W	0.7±0.1	3.14±0.07	22.8±10.3	[5.7; 1.8]
	W-Mo	0.5±0.1	3.14±0.07	22.8±10.3	
	W-W	0.5±0.1	3.16±0.01	4.9±1.0	

$Co_{1.1}$-$Mo_{0.28}$-$W_{0.72}$-s	Mo-Mo	0.0±0.03	3.15*	6.0*	
	Mo-W	1.0±0.03	3.16*	9.4±2.0	[3.6; 5.1]
	W-Mo	0.38±0.02	3.16*	9.4±2.0	
	W-W	0.62±0.02	3.15*	4.5*	

Table 6. Activities and selectivities of catalysts from simultaneous DBT HDS and THN HDA reactions.

Catalyst	r_{HDS}/mol(W+Mo) ($10^{-5}.s^{-1}$) [a]	r_{HDA}/mol(W+Mo) ($10^{-5}..s^{-1}$) [a]	*cis*-/*trans*-[b]	k_{BPH}/k_{DDS}[c]	k_{HYD}/k_{DD}[c]	r_{HDA}/r_{HDS}
$Ni_{1.6}$-Mo-s	88.1	28.8	0.9	0.11	1.5	0.3
$Ni_{1.9}$-$Mo_{0.62}$-$W_{0.38}$-s	73.3	32.1	0.7	0.12	1.7	0.4
$Ni_{1.7}$-$Mo_{0.50}$-$W_{0.50}$-s	67.8	27.7	0.5	0.17	1.6	0.4
$Ni_{1.5}$-$Mo_{0.32}$-$W_{0.68}$-s	72.3	42.2	0.5	0.18	1.9	0.6
$Ni_{1.6}$-W-s	60.3	42.6	0.5	0.35	1.7	0.7
$Co_{1.1}$-Mo-s	20.8	2.9	0.8	-	0.8	0.1
$Co_{1.2}$-$Mo_{0.69}$-$W_{0.31}$-s	37.3	6.7	0.8	-	0.6	0.2
$Co_{1.3}$-$Mo_{0.41}$-$W_{0.59}$-s	35.0	6.5	0.8	-	0.7	0.2
$Co_{1.1}$-$Mo_{0.28}$-$W_{0.72}$-s	34.4	3.5	0.7	-	0.7	0.1
$Co_{1.2}$-W-s	36.8	7.2	0.8	-	0.8	0.2
[d]$NiMo/Al_2O_3$	248	90.2	0.3	-	0.4	0.4

[a]r_{HDS} and r_{HDA} initial reaction rates for DBT HDS ($mol_{DBT}/mol_{(W+Mo).S}$) and THN HDA ($mol_{THN}/mol_{(W+Mo).S}$), respectively, per molar (W+Mo) metal content. [b]Selectivity ratio for THN HDA isomeric products from initial rates. [c] Selectivity for DBT HDS products determined from pseudo-first order kinetic model. [d] Ni/(Ni+Mo)=0.5; wt% Ni=4.1; wt% Mo=6.7, see [36].

References

[1] H. Topsøe, Clausen, B.S., and Massoth, F. E., Hydrotreating Catalysis Science and Technology, 1 ed., Springer-Verlag New York 1996.

[2] S. Eijsbouts, S.W. Mayo, K. Fujita, Appl. Catal. A:Gen, 322 (2007) 58-66.

[3] F.L. Plantenga, R. Cerfontain, S. Eijsbouts, F. van Houtert, G.H. Anderson, S. Miseo, S. Soled, K. Riley, K. Fujita, Y. Inoue, M.O.a.H.Y. Masakazu Anpo, Stud. Surf. Sci. Catal., Elsevier 2003, 407-410.

[4] S.L. Soled, Sabato, M.,Krycak, R., Vroman, H., Ho, T. e Riley, K., United State Patent, 6156695 (2000).

[5] S.L. Soled, Sabato, S.,Hou, Bulk Ni-Mo-W Catalysts made from precursors containing an organic agent, in: United State Patent (Ed.)US, 2009.

[6] H. Topsøe, R. Candia, N.-Y. Topsøe, B.S. Clausen, H. Topsøe, Bull. Soc. Chim. Belg., 93 (1984) 783-806.

[7] W. Eltzner, M. Breysse, M. Lacroix, C. Leclercq, M. Vrinat, A. Müller, E. Diemann, Polyhedron, 7 (1988) 2405-2409.

[8] M. Breysse, R. Frety, M. Lacroix, M. Vrinat, React. Kinet. Catal. Lett., 26 (1984) 97-101.

[9] M. Breysse, R. Frety, M. Vrinat, P. Grange, M. Genet, Appl. Catal. , 12 (1984) 165-178.

[10] P. Afanasiev, I. Bezverkhy, Chem. Mater., 14 (2002) 2826-2830.

[11] G. Alonso, G. Berhault, A. Aguilar, V. Collins, C. Ornelas, S. Fuentes, R.R. Chianelli, J. Catal., 208 (2002) 359-369.

[12] C. Thomazeau, C. Geantet, M. Lacroix, V. Harlé, S. Benazeth, C. Marhic, M. Danot, J. Solid State Chem., 160 (2001) 147-155.

[13] C. Thomazeau, C. Geantet, M. Lacroix, M. Danot, V. Harle, Oil Gas Sci. Technol. - Rev. IFP, 60 (2005) 781-790.

[14] C. Thomazeau, C. Geantet, M. Lacroix, M. Danot, V. Harlé, P. Raybaud, Appl. Catal. A: Gen., 322 (2007) 92-97.

[15] D. Genuit, P. Afanasiev, M. Vrinat, J. Catal., 235 (2005) 302-317.

[16] Y. Gochi, C. Ornelas, F. Paraguay, S. Fuentes, L. Alvarez, J.L. Rico, G. Alonso-Núñez, Catal. Today, 107-108 (2005) 531-536.

[17] L. Wang, Y. Zhang, Y. Zhang, Z. Jiang, C. Li, Chem.– A Eur. J., 15 (2009) 12571-12575.

[18] L. van Haandel, M. Bremmer, P.J. Kooyman, J.A.R. van Veen, T. Weber, E.J.M. Hensen, ACS Catal., 5 (2015) 7276-7287.

[19] M. Ramos, G. Berhault, D.A. Ferrer, B. Torres, R.R. Chianelli, Catal. Sci. & Technol., 2 (2012) 164-178.

[20] N. Hermann, M. Brorson, H. Topsoe, Catal. Lett., 65 (2000) 169-174.

[21] B. Yoosuk, J.H. Kim, C. Song, C. Ngamcharussrivichai, P. Prasassarakich, Catal. Today, 130 (2008) 14-23.

[22] J. Ren, A. Wang, J. Tan, G. Cao, C. Liu, Y. Li, M. Lu, Y. Hu, S.Q.Y.T.a.C.Y. Dongyuan Zhao, Stud. Surf. Sci. Catal., Elsevier2007, pp. 721-724.

[23] H. Farag, J. Colloids Interface Sci., 348 (2010) 219-226.

[24] V. Rabarihoela-Rakotovao, S. Brunet, G. Perot, F. Diehl, Appl. Catal. A:Gen., 306 (2006) 34-44.

[25] D.D. Whitehurst, T. Isoda, I. Mochida, W.O.H.B.G.a.H.K.z. D.D. Eley, Adv. Catal., Academic Press1998, pp. 345-471.

[26] Y. Iwata, Y. Araki, K. Honna, Y. Miki, K. Sato, H. Shimada, Catal. Today, 65 (2001) 335-341.

[27] T. Isoda, K. Kusakabe, S. Morooka, I. Mochida, Energy Fuels, 12 (1998) 493-502.

[28] H. Farag, I. Mochida, J. Colloid Interface Sci., 372 (2012) 121-129.

[29] C. Leyva, M.S. Rana, F. Trejo, J. Ancheyta, Catal. Today, 141 (2009) 168-175.

[30] J. Hein, O.Y. Gutiérrez, E. Schachtl, P. Xu, N.D. Browning, A. Jentys, J.A. Lercher, ChemCatChem, 7 (2015) 3692-3704.

[31] Y.E. Licea, S.L. Amaya, A. Echavarria, J. Bettini, J.G. Eon, L.A. Palacio, A.C. Faro, Catal. Sci. Technol., 4 (2014) 1227-1238.

[32] S. Mitchell, A. Gómez-Avilés, C. Gardner, W. Jones, J. Solid State Chem., 183 (2010) 198-207.

[33] F.A. Cotton, G. Wilkinson, Advanced Inorganic Chemistry: a comprehensive text, Interscience Publishers 1966.

[34] A.V. Sapre, B.C. Gates, Ind. Eng. Chem. Proc. DD, 20 (1981) 68-73.

[35] B.C. Gates, H. Topsøe, Polyhedron, 16 (1997) 3213-3217.

[36] A.S. Rocha, A.C. Faro Jr, L. Oliviero, J. Van Gestel, F. Maugé, J. Catal., 252 (2007) 321-334.

[37] E.P. Barrett, L.G. Joyner, P.P. Halenda, J. Am. Chem. Soc., 73 (1951) 373-380.

[38] M. Newville, J Synchrotron Radiat., 8 (2001) 322-324.

[39] A.L. Ankudinov, B. Ravel, J.J. Rehr, S.D. Conradson, Phys. Rev. B, 58 (1998) 7565-7576.

[40] R. Grau-Crespo, S. Hamad, C.R.A. Catlow, N.H. de Leeuw, J Phys-Condens Mat, 19 (2007).

[41] G. Kresse, J. Furthmüller, Phys. Rev. B, 54 (1996) 11169-11186.

[42] G. Kresse, J. Furthmüller, Comput. Mater. Sci., 6 (1996) 15-50.

[43] P.E. Blöchl, Phys. Rev. B, 50 (1994) 17953-17979.

[44] G. Kresse, D. Joubert, Phys. Rev. B, 59 (1999) 1758-1775.

[45] D. Levin, S.L. Soled, J.Y. Ying, Inorg. Chem., 35 (1996) 4191-4197.

[46] S.L. Soled, Sabato, M.,Krycak, R., Vroman, H., Ho, T. e Riley, K., United State Patent, 7288182B1 (2007), 2000.

[47] D. Levin, J.Y. Ying, 3rd World Congress on Oxidation Catalysis1997, pp. 367-373.

[48] L.M. Madeira, M.F. Portela, C. Mazzocchia, Catal. Rev., 46 (2004) 53-110.

[49] S.M.A.M. Bouwens, D.C. Koningsberger, V.H.J. De Beer, S.P.A. Louwers, R. Prins, Catal. Lett., 5 (1990) 273-283.

[50] S.P.A. Louwers, R. Prins, J. Catal., 133 (1992) 94-111.

[51] S.P.A. Louwers, R. Prins, J. Catal., 139 (1993) 525-539.

[52] S.D. Kelly, N. Yang, G.E. Mickelson, N. Greenlay, E. Karapetrova, W. Sinkler, S.R. Bare, J. Catal., 263 (2009) 16-33.

[53] S.P.A. Louwers, M.W.J. Craje, A.M. Vanderkraan, C. Geantet, R. Prins, J. Catal., 144 (1993) 579-596.

[54] S.D. Kelly, B. Ravel, AIP Conf. Proc., 882 (2007) 132-134.

[55] B. Ravel, M. Newville, J. Synchrotron Radiat., 12 (2005) 537-541.

[56] J. Corps, P. Vaqueiro, A. Aziz, R. Grau-Crespo, W. Kockelmann, J.-C. Jumas, A.V. Powell, Chem. Mater., 27 (2015) 3946-3956.

[57] R. Grau-Crespo, N.H. De Leeuw, S. Hamad, U.V. Waghmare, Proc. Royal Soc. A-Math. Phys. Eng. Sci., 467 (2011) 1925-1938.

[58] Q. Wang, R. Grau-Crespo, N. H de Leeuw, J. Phys. Chem. B., 115 (2011) 13854-13861.

[59] F. Bataille, J.L. Lemberton, G. Pérot, P. Leyrit, T. Cseri, N. Marchal, S. Kasztelan, Appl. Catal. A:Gen., 220 (2001) 191-205.

[60] H. Yasuda, M. Higo, S. Yoshitomi, T. Sato, M. Imamura, H. Matsubayashi, H. Shimada, A. Nishijima, Y. Yoshimura, Catal. Today, 39 (1997) 77-87.